Digital three-dimensional image correlation by use of computer-reconstructed integral imaging

Yann Frauel and Bahram Javidi

We use integral images of a three-dimensional (3D) scene to estimate the longitudinal depth of multiple objects present in the scene. With this information, we digitally reconstruct the objects in three dimensions and compute 3D correlations of input objects. We investigate the use of nonlinear techniques for 3D correlations. We present experimental results for 3D reconstruction and correlation of 3D objects. We demonstrate that it is possible to perform 3D segmentation of 3D objects in a scene. We finally present experiments to demonstrate that the 3D correlation is more discriminant than the two-dimensional correlation. © 2002 Optical Society of America

OCIS codes: 110.6880, 100.6890, 100.5010, 110.4190.

1. Introduction

The area of three-dimensional (3D) object acquisition and visualization[1] has been researched for many years, by use of holography,[2,3] integral photography,[4–10] or other techniques.[11–13] Recently researchers tried to extend the traditional two-dimensional (2D) pattern-recognition application[14–18] to 3D objects. One possibility that was investigated is recognition performance by use of digital holograms of the 3D objects.[19–21] However, this technique requires coherent illumination. Other methods involve the use of several perspectives of the objects.[22–24] These perspectives are usually obtained by one moving either the object or the camera. Integral imaging[4] provides a convenient way to acquire simultaneously several 2D perspectives of a 3D scene. In this technique many images of a 3D object are obtained with a microlens array and recorded by a camera. Each elementary image gives a slightly different perspective of the 3D object depending on the location of the corresponding microlens relative to the object. A proposal was made to apply this kind of integral imaging to 3D object recognition.[25] This technique has the advantage of offering the possibility of an all-optical implementation. However, it relies on a classical 2D correlator architecture and cannot deal with precise longitudinal segmentation of the 3D objects.

In this paper we propose a new technique based on integral imaging for recognizing and locating 3D objects in a 3D scene. This technique computes actual 3D correlations between digitally reconstructed 3D objects. In Section 1 we will describe briefly the principle of integral imaging. In Section 2 we will explain how we extract from integral images the information about the depth of the 3D object. We show how to digitally reconstruct the 3D scene in the computer. In Section 3 we will describe the computation of the 3D correlation, and, finally, in Section 4 we will provide optical experimental results.

2. Description and Acquisition of an Integral Image

Our experimental setup is presented in Fig. 1. The main component is an hexagonal microlens array that is placed in front of the 3D scene to be analyzed. The microlenses have diameters of $\phi = 200$ μm and focal lengths around 2.3 mm. Each of these microlenses generates a small image of the scene taken from a different point of view. We make the following assumptions:

1. The depth of focus of the microlenses is sufficient to assume that the images of all the objects are obtained in the same plane P independently from their longitudinal position in the 3D scene.

The authors are with the Department of Electrical and Computer Engineering, University of Connecticut, 260 Glenbrook Road, U-157, Storrs, Connecticut 06269-2157. Y. Frauel is also with the Instituto de Investigaciones en Matemáticas Aplicades y en Sistemas, Universidad Nacional Autónoma de México, Apdo. Postal 20-726 Admon. No. 20, Delegación de Alvaro Obregón, 01000 México, D.F., México. B. Javidi's e-mail address is Bahram@engr.uconn.edu.

Received 10 January 2002; revised manuscript received 5 June 2002.

0003-6935/02/265488-09$15.00/0

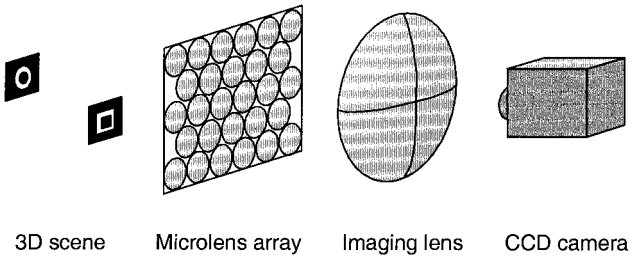

Fig. 1. Experimental setup.

2. The elementary images generated by the microlenses do not overlap each other.

These conditions can always be obtained by placing the objects sufficiently far from the microlenses. In this case, all the images are obtained in a plane P at distance $d \approx f$ from the array (Fig. 2). This plane is then imaged by an additional lens onto a CCD camera. Except for a magnification coefficient—and some amount of aberrations that we will neglect—the image obtained at the camera is identical to the one obtained in the imaging plane P of the microlens array. We will therefore neglect this last imaging step, and we will conduct all the calculations in plane P.

As can be seen in Fig. 2, the coordinate X_p of an object point projected in plane P by the microlens number p depends on the original coordinate x of the object point as well as on its depth z, according to the following:

$$\frac{p\phi - x}{z} = \frac{X_p - p\phi}{d}, \tag{1}$$

which yields

$$X_p = p\phi\left(1 + \frac{d}{z}\right) - \frac{d}{z}x. \tag{2}$$

Of course, the same formula is obtained with the coordinate y. This relation is illustrated in Fig. 3 for X_0 ($p = 0$). The distance between the projections of

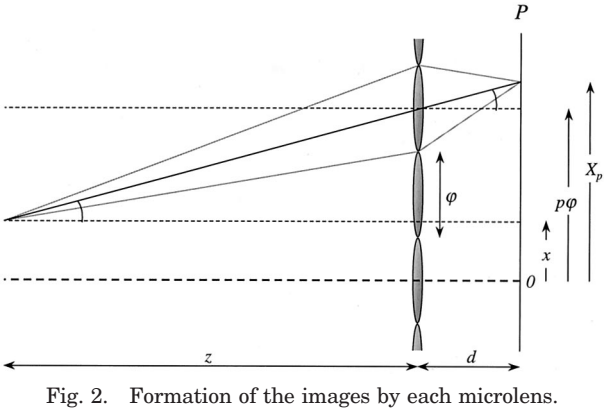

Fig. 2. Formation of the images by each microlens.

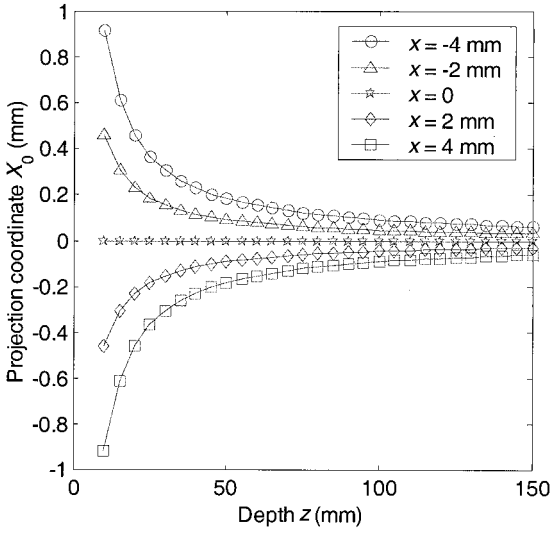

Fig. 3. Displacement of the projected object point versus depth of the object point for the central microlens.

the same object point given by two microlenses p and q is

$$X_q - X_p = (q - p)\phi\left(1 + \frac{d}{z}\right). \tag{3}$$

Thus the depth of a given object point can be recovered by comparison of the projections through different microlenses. This is a triangulation technique. The first step is therefore to acquire an image of plane P that contains several elementary images provided by every microlens. To improve the quality of this image, we digitally enhance its contrast. Moreover, as we do not know the magnification ratio between plane P and the camera, we also need to calibrate our images. We do this by illuminating the microlens array with a uniform plane wave produced by a He–Ne laser. We thus obtain an image with focused spots that provide the locations—in pixels—of the centers of the microlenses.

3. Three-Dimensional Reconstruction of the Objects

In this section we describe how to extract the 3D scene depth information from the set of 2D elementary images acquired at the first step. We then use this information to generate a 3D reconstruction of the object by computer.

A. Retrieval of the Three-Dimensional Scene Depth

It can be seen in Eq. (3) that two elementary images would, in principle, be sufficient to determine the depth z of every point (stereoscopy). However, the main problem is to find the correspondence between the points of different elementary images. Namely, to measure the projected coordinates X_p, we need to know which point in each elementary image corresponds to the original object point. The correspondences of the projected points can be determined by comparison of several elementary images. Com-

pared with mere stereoscopic pairs, our integral images have the advantage of providing not only two but several perspectives of the 3D object. Because the feature matching between two images can be ambiguous, the use of several images helps to determine which points of the different views actually correspond to each other. According to Eq. (3), one particular feature has to appear at regular locations among the various elementary images. A distinct object feature, even if it accidentally appears similar to the first elementary image, will not appear in consistent locations [in terms of Eq. (3)] in all the elementary images. Thus the use of several views allows a more accurate identification of the features and therefore a better determination of the depth. Moreover, some elementary images may present noise that is due to defective pixels of the detector or noise in the optical system. In this case, the use of many images provides redundancy that lowers the effect of noise. However, the camera has a fixed number of pixels and increasing the number of elementary images obviously reduces the resolution of each of them, hence reducing the lateral resolution of the reconstructed 3D object. Moreover, increasing the number of elementary images increases the computational load for determining the depth of each point. In our experiment the size and number of elementary images were dictated by the available optical components. Figure 4 shows an example of our integral images. With our particular configuration, we found out heuristically that using only 7×7 of the elementary images (Fig. 4) was a good trade-off between computation time and accuracy of the depth estimation. The optimum number of images may vary with the configuration and components used.

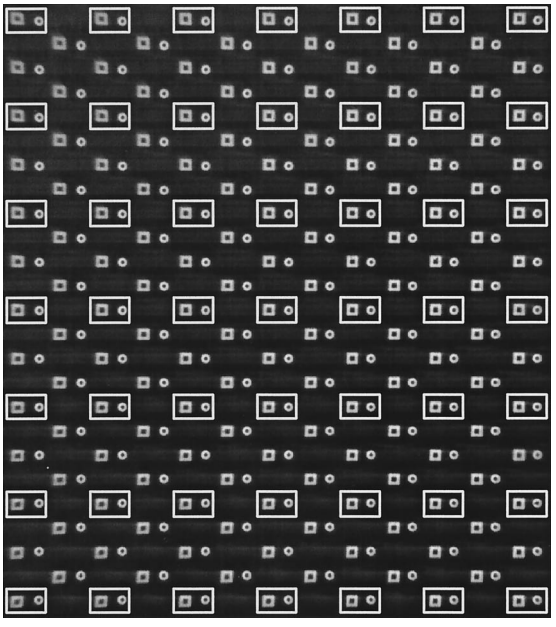

Fig. 4. Example of integral image of a 3D scene. The elementary images marked are the ones used for determining the scene depth.

To find the depth of the object points, we use a stereo-matching algorithm.[10] Let us consider one particular point of the central elementary image—the one corresponding to the microlens (0, 0). If we choose its depth z arbitrarily, we can determine the corresponding points in the other elementary images according to Eq. (3). We now need to verify that these points are actual projections of the same object point. This cannot be done by our comparing only one point to another. We need to compare the surroundings of each of these points. To do that, we compute the normalized 2D cross correlations between pairs of 9×9 pixel windows centered on the tested points. If I denotes the integral image, the projection of the inspected object point corresponding to the microlens (p, q) is $I(X_p, Y_q)$. The normalized cross correlation between the window contained in the elementary image (p, q) and the one contained in the elementary image (p', q') is

$$C[(p, q), (p', q')] = \frac{\sum_{m=-4}^{4} \sum_{n=-4}^{4} I(X_p + m, Y_q + n) I(X_{p'} + m, Y_{q'} + n)}{\left[\sum_{m=-4}^{4} \sum_{n=-4}^{4} I^2(X_p + m, Y_q + n) \sum_{m=-4}^{4} \sum_{n=-4}^{4} I^2(X_{p'} + m, Y_{q'} + n) \right]^{1/2}}. \quad (4)$$

This similarity criterion has the advantage of being independent of the intensity variations that can occur between two elementary images. We compare each window with all of its immediate neighbors (horizontally and vertically), and we add together all the correlation values. This gives us a matching criterion that we need to maximize:

$$M(z) = \sum_{p=-3}^{3} \sum_{q=-2}^{3} C[(p, q-1), (p, q)] + \sum_{q=-3}^{3} \sum_{p=-2}^{3} C[(p-1, q), (p, q)]. \quad (5)$$

We can compute the value of this criterion for a range of assumed depths z with a sample step of 1 mm, for instance. The depth (z value) that provides the highest value for $M(z)$ is the actual depth of the point under consideration. Actually, owing to the pixelization and the imperfections of the integral image, the curve of $M(z)$ presents some irregularities that can generate errors in the localization of the maximum value [Fig. 5(a)]. Fortunately, the global

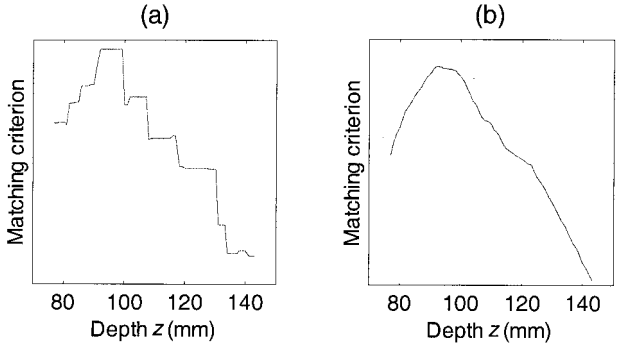

Fig. 5. Matching criterion [see Eq. (5)] versus depth. (a) Without filtering and (b) with convolution by a 15-mm-wide filter.

shape of the curve is always smooth, so that we can reduce the irregularities by applying a low-pass filter. Figure 5(b) shows the same curve as Fig. 5(a) convolved by a 15-sample-wide (15-mm) gate function. Because the new curve is more regular, its maximum can be used to find the depth of the projected point under consideration. Although this low-pass filtering may not avoid an unbiased estimate of the maximum, it does eliminate accidental peaks that are due to the imperfections of the images. This procedure is repeated for every point of the central elementary image to obtain the depth of every point for the 3D scene.

The criterion $M(z)$ is initially computed at every millimeter. However, the standard deviation of the measured depths of various points indicates that the accuracy of the z measurement is only approximately 10 mm. This is related to the pixelization of the integral image, which introduces a limit on lateral resolution and therefore on longitudinal resolution as well. Owing to the principle of triangulation, for a given setup the longitudinal resolution is lower for distant objects than for closer ones (see Fig. 3). Here the value of 10 mm is due to our particular components and distances of the objects. To reflect the actual accuracy of the depth measurement, we increase the quantization step of the measurement from 1 to 10 mm. Namely, the previous values of z are rounded to the nearest multiple of 10 mm. Indeed, because the resolution is not higher than 10 mm, it is pointless to keep intermediate planes that are not significant. In other words, we are able to reconstruct the object volume with a voxel depth no smaller than 10 mm. We thus need to assign—by rounding the z values—each reconstructed point to one of these voxels. Actually, keeping the intermediate planes would introduce noise (that is, fluctuations of the measurement depth) that would reduce the correlation peaks (see Section 4). A further study could determine the optimal step for estimating the depth.

B. Correction of the Depth-Dependent Magnification Ratio

In Subsection 3.A we described how to compute the z coordinate of each point of the central elementary image. However, for each of these points, we know only the projected coordinates X_0 and Y_0, and we need to find their actual coordinates x and y in the object space to reconstruct the 3D object. Knowing their depth z, we can do this by using Eq. (2), which yields

$$x = -(z/d)X_0, \qquad y = -(z/d)Y_0. \tag{6}$$

These equations compensate for the well-known fact that distant objects appear smaller in an image plane. By using Eqs. (6), we can reconstruct their size independently of their distances from the microlens array. At this stage we obtain a 3D reconstruction of the object space, and this 3D scene can be used to perform 3D image processing such as correlations. We can threshold the reconstructed 3D scene to remove the background noise before computing the 3D correlation.

4. Three-Dimensional Image Correlation

If $A(x, y, z)$ and $B(x, y, z)$ are two 3D objects, we define their similarity as the square modulus of their 3D correlation. We compute it through the Fourier domain:

$$S_{AB} = |A \otimes B|^2 = |\mathrm{FT}^{-1}(\tilde{A}\tilde{B}^*)|^2, \tag{7}$$

where the symbol $\otimes$ stands for the 3D correlation, $\tilde{A}$ and $\tilde{B}$ are the Fourier transforms of A and B, respectively, and FT^{-1} is the inverse Fourier transform. Moreover, to improve the recognition performance, we can use the kth-law nonlinear correlation[18] that provides us with the degree of similarity:

$$S_{AB}^{\ k} = |A \underset{k}{\otimes} B|^2 = |\mathrm{FT}^{-1}[|\tilde{A}|^k \exp(i\phi_{\tilde{A}})|\tilde{B}|^k \exp(-i\phi_{\tilde{B}})]|^2, \tag{8}$$

where $|\tilde{A}|$ and $|\tilde{B}|$ are the moduli of $\tilde{A}$ and $\tilde{B}$, respectively, and $\phi_{\tilde{A}}$ and $\phi_{\tilde{B}}$ are their arguments. The value of the nonlinear factor k is usually chosen between 0 and 1. The linear similarity described in Eq. (7) is obtained for $k = 1$. Using a strong nonlinearity—which means k is close to 0—improves the discrimination between similar objects. However, in this case, the recognition also becomes more sensitive to distortions of the objects. Namely, an object is not properly recognized if it is reconstructed with errors in the depth estimation. This is due to the fact that it does not exactly look like the reference anymore whereas the system is extremely discriminant. It is thus essential that all the points that are at the same distance from the microlens array are not found to be at different distances. This is the reason why, as we mentioned in Section 3, it is better to reduce the quantization step of the depth, provided that we estimate the same depth for all the points that are actually at the same distance. In the following, we will use the term correlation to designate the similarity criteria defined in Eqs. (7) and (8).

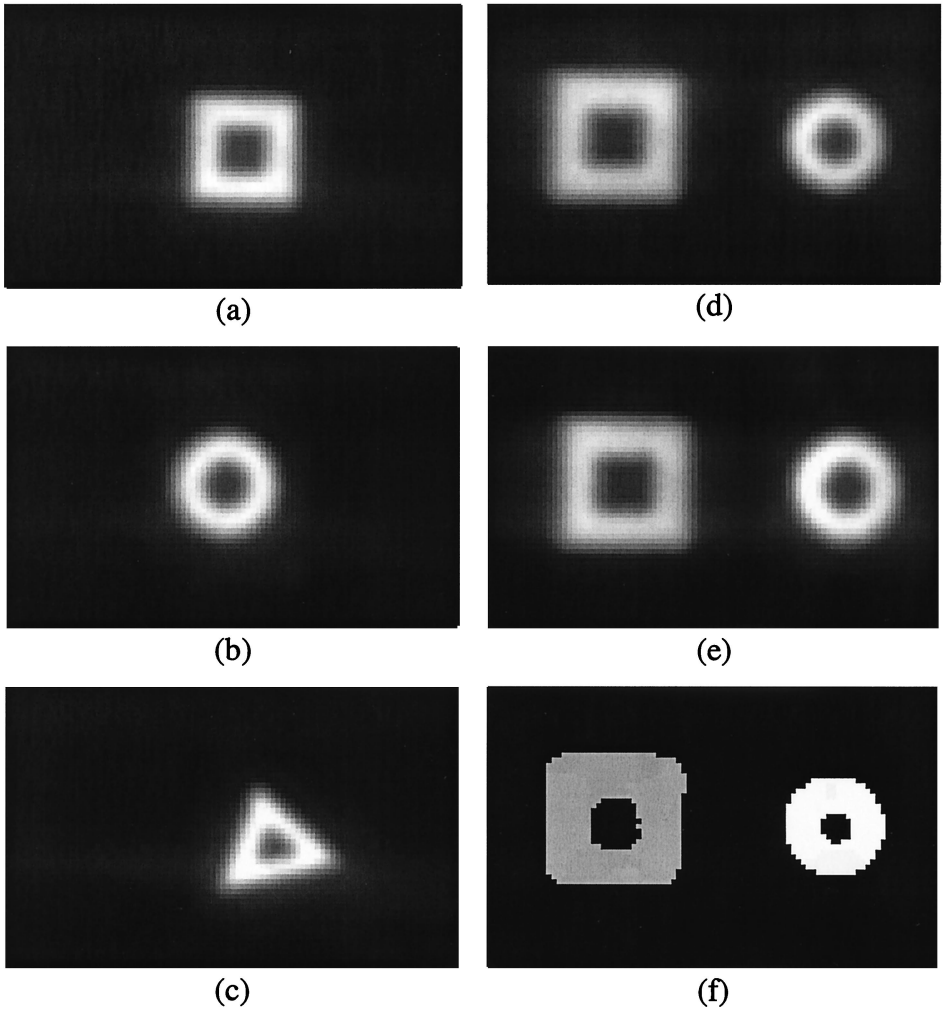

Fig. 6. Views of the 3D objects used in the experiments. (a), (b), and (c) 3D reference objects; (d) and (e) 3D input scenes with the reference objects at various distances from the detector; (f) map of the estimated depths for the 3D scene shown in (d).

5. Experimental Results

In this section we present experiments for 3D reconstruction and recognition of objects from experimental integral images. Nonlinear correlation techniques are presented to recognize and locate a 3D object in the 3D input scene. The experiments demonstrate the greater recognition and discrimination capability of 3D correlation over 2D correlation.

A. Acquisition and Reconstruction of the Three-Dimensional Scenes

In the experiments, three planar objects representing three different geometrical shapes, namely, a square, a circle, and a triangle, are used. These shapes are approximately 2 mm large and are located between 90 and 120 mm from the microlens array. The three objects are shown in Figs. 6(a)–6(c). These images are the central elementary images generated by the microlens array. We create two 3D scenes by placing the square and the circle at various distances from the array. These scenes can be seen in Figs. 6(d) and 6(e). We call scene 1 the scene in Fig. 6(d) and scene 2 the scene in Fig. 6(e). Although they look similar, the perspective views in Figs. 7(a) and 7(b) show the difference in depth. In scene 1 the circle is located farther from the square. This explains its smaller size in Fig. 6(d) compared with Fig. 6(e). Figure 6(f) provides a map of the distances obtained by the matching algorithm (see Section 2) for scene 1. The brighter points correspond to larger distances of z. The points whose intensity is below the threshold have been plotted in black.

Figure 8 illustrates the 3D reconstructions of scene 1 and scene 2. The contrast has been inverted for better visualization. It can be noted that, owing to the use of Eq. (6), the circle is now the same size as the square, which was not the case in Figs. 6(d) and 6(e). The absolute depth of the objects is estimated with an accuracy better than 10 mm. The errors can be due to a wrong estimation value of the distance d between the microlens array and the projection plane P or to a poor estimation of the location of the centers of the microlenses.

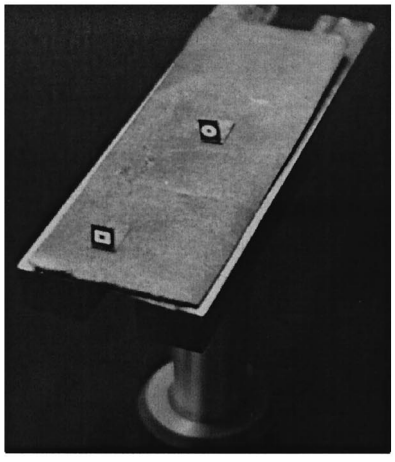

(a)

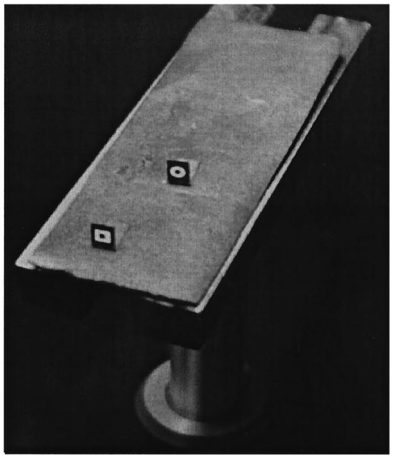

(b)

Fig. 7. Perspective views of the 3D scenes used in the experiments. (a) Scene 1 and (b) scene 2.

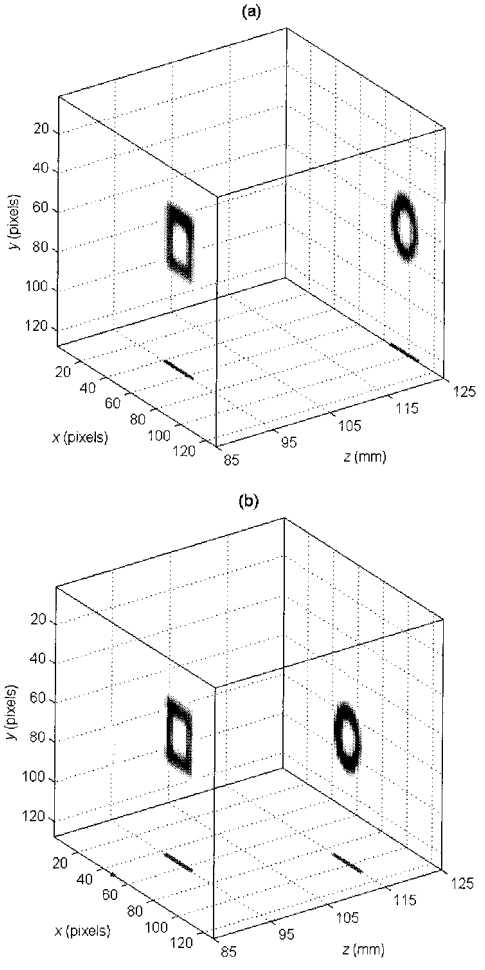

Fig. 8. Three-dimensional representation of the reconstructed scenes. (a) Scene 1 and (b) scene 2.

B. Detection of a Three-Dimensional Object by Use of Nonlinear Correlation

To study the recognition and discrimination capability of the proposed system, we first consider the two composite scenes (scene 1 and scene 2) as the 3D inputs to be tested. The three single geometrical objects (square, triangle, and circle) are used as the 3D reference objects. The 3D correlations between each input scene and each reference object is computed, which provides $2 \times 3 = 6$ correlations. For each of these correlations, we obtain two main peaks that correspond to the two objects present in both input scenes. Thus $2 \times 6 = 12$ peaks are generated, among which only four are considered as detection peaks: the ones corresponding to the square in both scenes when the square is used as a reference and the ones corresponding to the circle in both scenes when the circle is used as a reference. All the other peaks are undesirable. We illustrate the effect of kth-law nonlinear correlation[18] on the values of these peaks as a function of the nonlinear factor k. We determine the relative values of the different peaks for each particular value of k. A different normalization factor is applied for every k, so that one of the four detection peaks is always unity. Figure 9 illustrates the normalized peak values versus k. It is evident from this graph that it is possible to separate detection peaks from undesirable peaks if $k \leq 0.5$. A linear correlation is thus excluded. It can be seen that the best discrimination is obtained for $k = 0.2$. For this value of the nonlinear factor, it is easy to find a threshold that will allow us to discriminate between detection peaks and undesirable peaks.

To confirm these results, we consider the correlations of scene 1 or scene 2 with a reference object (square or circle) that is present in the scene. For each of these correlations, we obtain two peaks: a detection peak P_D and an undesirable peak P_U. We define the discrimination factor as $\mathrm{DF} = P_D/P_U$. The correct recognition can take place only if $\mathrm{DF} > 1$. The plot of this discrimination factor versus k is shown in Fig. 10 for each of the correlations. It is evident that nonlinear correlation is required to detect the 3D objects.

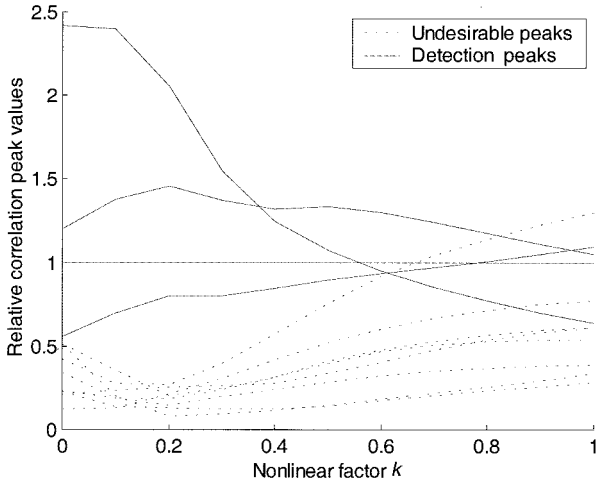

Fig. 9. Normalized values of the correlation peaks versus the kth-law nonlinearity. The detection peaks are the ones corresponding to the presented reference object. The other peaks are undesirable (false alarms).

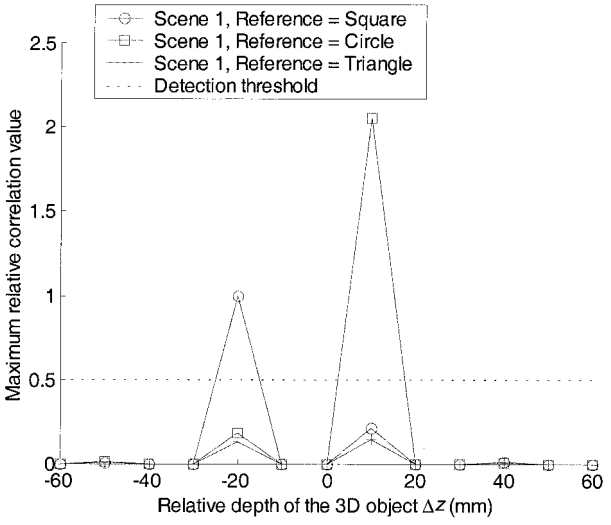

Fig. 11. Segmentation of the depth of the detected 3D objects.

C. Three-Dimensional Localization of an Object

In the experiment described in Subsection 5.B, a correlation peak was obtained for each object in the 3D input scene. This peak is obviously 3D and indicates the 3D location of the object in the input scene relative to the location of the object in the reference scene. For instance, Fig. 11 presents the maximum correlation values at every depth when we correlate scene 1 with the three 3D reference objects. A nonlinear correlation with $k = 0.2$ is used. As mentioned in Subsection 5.B, the detection peaks are selected by application of a threshold to the output at 0.5. The relative locations Δz of the remaining peaks indicate the longitudinal depths of the corresponding objects.

Figure 12 illustrates the correlation planes with fixed z at which the maximum peaks for the square reference are generated. This graph demonstrates that the relative (x, y, z) locations of the objects can be found by the positions of the peaks. In this example, the peak in Fig. 12(b) would not be taken into consideration because it is below the threshold.

We present an additional illustration of the 3D localization of the objects. Figure 13 presents the volume representation of the 3D correlation between scene 1 and both the square reference object [Fig. 13(a)] and the circle reference object [Fig. 13(b)]. The detection peaks are plotted in 3D. They provide the relative 3D coordinates of the reference objects in the input scene.

D. Comparison between Two-Dimensional and Three-Dimensional Correlation

In the previous subsections we achieved 3D detection of elementary objects (a square and a circle) in complex 3D scenes (scene 1 and scene 2). In this subsection we compare two complex scenes to each other. Scene 1 and scene 2 have different 3D structures. They therefore constitute two different 3D objects. The correlation of these two 3D objects will be compared by use of conventional correlation of 2D images and by proposed 3D correlation. The 2D correlation is obtained between the images shown in Figs. 6(d)

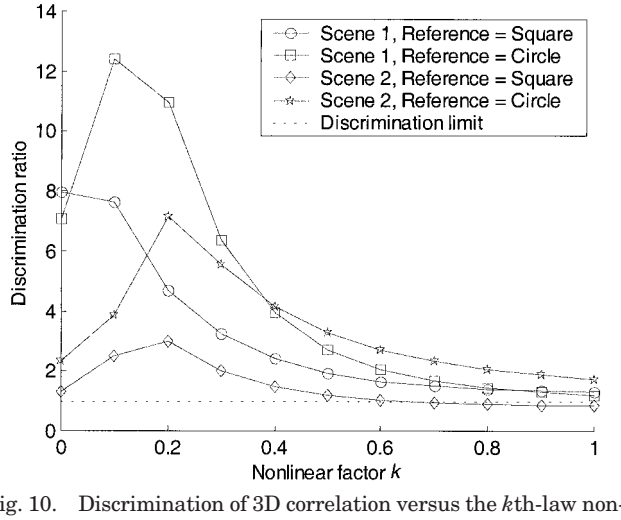

Fig. 10. Discrimination of 3D correlation versus the kth-law nonlinearity.

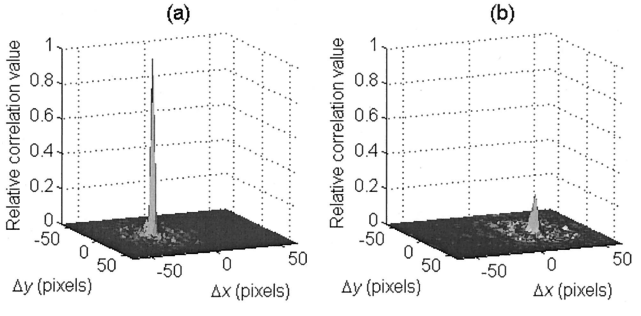

Fig. 12. Two correlation planes extracted from the 3D correlation between scene 1 and the 3D square reference object. (a) Correlation plane corresponding to $\Delta z = -20$ mm and (b) correlation plane corresponding to $\Delta z = +10$ mm.

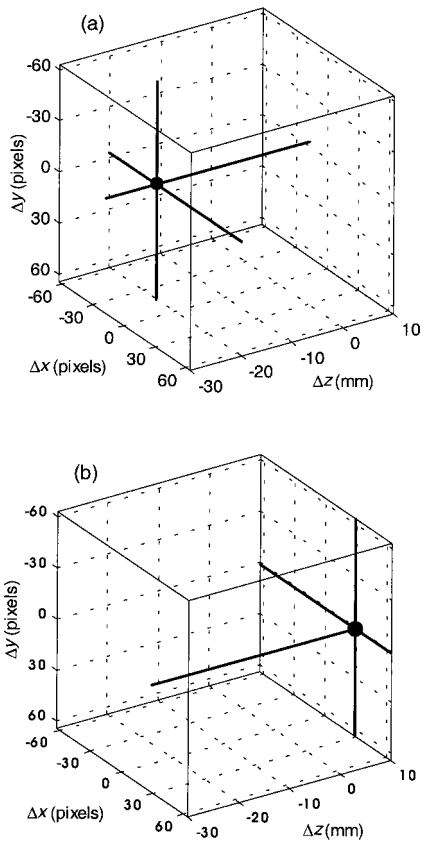

Fig. 13. Three-dimensional representation of the correlation volumes. (a) Scene 1, square reference and (b) scene 1, circle reference.

and 6(e), which are the views obtained through the central microlens of the array. We apply a thresholding on the images to remove the background noise. The second comparison method consists in digitally reconstructing the 3D scenes and computing their 3D correlation as described previously. The values $C_{1\text{-}2}$ of the cross-correlation peaks for both of these methods are given in Table 1. In both cases (2D or 3D), we use a nonlinear correlation with $k = 0.2$. Of course, the correlation values by themselves cannot be compared because they are not normalized. To give a comparison scale, we also provide the values of the autocorrelations for scene 1 ($C_{1\text{-}1}$) and scene 2 ($C_{2\text{-}2}$) for both the 2D and the 3D methods. Last, analogous to what we did in Subsection 5.B, we define the discrimination ratio as the ratio between the value of the autocorrelation and the value of the cross correlation. Table 1 presents the values of this ratio with respect to both scenes. It can be seen that the 3D correlation is roughly three times more discriminant than the 2D correlation. This is because it takes into account some additional information concerning the depth structure of the 3D objects.

Table 1. Comparison between 2D and 3D Correlations for Discriminating between Two 3D Objects

Correlation	$C_{1\text{-}2}$	$C_{1\text{-}1}$	$C_{2\text{-}2}$	$C_{1\text{-}1}/C_{1\text{-}2}$	$C_{2\text{-}2}/C_{1\text{-}2}$
2D	0.157	1.29	1.33	8.2	8.5
3D	1.74×10^9	36.0×10^9	47.5×10^9	21	27

6. Conclusion

In this paper we have demonstrated the digital reconstruction and recognition of 3D objects by using integral imaging. First, we recalled how it is possible to estimate the depth of an object from an integral image by using a triangulation technique. Then we used this depth information to digitally reconstruct the objects in three dimensions. With these reconstructed 3D objects, we performed numerical 3D correlations in order to recognize the 3D objects. We presented nonlinear correlation results using various nonlinearities to investigate the discrimination capability. It was demonstrated that the proposed technique may be used to recognize and locate 3D objects in a 3D scene. Although the depth resolution is presently low (approximately 10 mm for our experiments), it could be increased by improvement of the quality of the integral images. These improvements depend on the optical aberrations and distortion, number of pixels of the detector, and number of the microlenses. Further improvement could be obtained through better estimation of the parameters of the system such as location of the microlenses and distance between the array and the image plane. Finally, it was shown that the 3D correlation provides a better discrimination than 2D correlation because it uses the object depth information. The proposed 3D recognition technique is shift invariant; that is, it is not affected by a lateral or longitudinal shift of the 3D object. A remaining problem is the handling of hidden parts. If a part of an object is visible in one elementary image but occluded in another one, the depth estimation may be impaired. In that case, it might be interesting to take advantage of the multiplicity of elementary images provided by integral photography. This could be done by detection of whether a particular feature is present on all the views or only on a subset of them. In the latter case, the depth estimation could take place by use of only this subset. This proposal could be the subject of future research.

The authors are grateful to M. R. Taghizadeh, at Heriot-Watt University in Edinburgh, for providing the microlens array. They also thank Thomas Naughton for his careful reading of this manuscript, as well as the reviewers for their useful comments.

References

1. B. Javidi, ed., *3D Television, Video, and Digital Technologies* (Springer-Verlag, Berlin, 2002).
2. E. N. Leith and J. Upatniecks, "Reconstructed wavefronts and communication theory," J. Opt. Soc. Am. **52,** 1123–1130 (1962).
3. J. Caulfield, *Handbook of Optical Holography* (Academic, London, 1979).
4. G. Lippmann, "La photographic intégrale," C. R. Acad. Sci. **146,** 446–451 (1908).

5. F. Okano, J. Arai, H. Hoshino, and I. Yuyama, "Three-dimensional video system based on integral photography," Opt. Eng. **38,** 1072–1077 (1999).
6. S. Nakajima, K. Masamune, I. Sakuma, and T. Dohi, "Three-dimensional display system for medical imaging with computer-generated integral photography," in *Stereoscopic Displays and Virtual Reality Systems VII*, J. O. Merritt, S. A. Benton, A. J. Woods, and M. T. Bolas, eds., Proc. SPIE **3957,** 60–67 (2000).
7. H. Arimoto and B. Javidi, "Integral three-dimensional imaging with digital reconstruction," Opt. Lett. **26,** 157–159 (2001).
8. T. Okoshi, *Three-Dimensional Imaging Techniques* (Academic, New York, 1971).
9. S.-W. Min, S. Jung, J.-H. Park, and B. Lee, "Three-dimensional display system based on computer-generated integral photography," in *Stereoscopic Displays and Virtual Reality Systems VIII*, A. J. Woods, M. T. Bolas, J. O. Merritt, and S. A. Benton, eds., Proc. SPIE **4297,** 187–195 (2001).
10. J.-H. Park, S.-W. Min, S. Jung, and B. Lee, "New stereovision scheme using a camera and a lens array," in *Algorithms and Systems for Optical Information Processing V*, B. Javidi and D. Psaltis, eds., Proc. SPIE **4471,** 73–80 (2001).
11. N. Mayer and R. Sand, "Stereoscopic television," Rundfunktech. Mitt. **13,** 123–134 (1969).
12. T. Motoki, H. Isono, and I. Yuyama, "Recent status of 3-dimensional television research," Proc. IEEE **83,** 1009–1021 (1995).
13. A. R. L. Travis, "Display of three-dimensional video images," Proc. IEEE **85,** 1817–1832 (1997).
14. A. B. VanderLugt, "Signal detection by complex spatial filtering," IEEE Trans. Inf. Theory **10,** 139–145 (1964).
15. J. W. Goodman, *Introduction to Fourier Optics* (McGraw-Hill, New York, 1968).
16. Ph. Réfrégier, "Filter design for optical pattern recognition: multicriteria optimization approach," Opt. Lett. **15,** 854–856 (1990).
17. B. Javidi, ed., *Image Recognition Classification* (Marcel Dekker, New York, 2002).
18. B. Javidi, "Nonlinear joint power spectrum based optical correlation," Appl. Opt. **28,** 2358–2367 (1989).
19. B. Javidi and E. Tajahuerce, "Three-dimensional object recognition by use of digital holography," Opt. Lett. **25,** 610–612 (2000).
20. Y. Frauel, E. Tajahuerce, M. A. Castro, and B. Javidi, "Distortion-tolerant three-dimensional object recognition with digital holography," Appl. Opt. **40,** 3887–3893 (2001).
21. Y. Frauel and B. Javidi, "Neural network for three-dimensional object recognition based on digital holography," Opt. Lett. **26,** 1478–1480 (2001).
22. A. Pu, R. Denkewalter, and D. Psaltis, "Real-time vehicle navigation using a holographic memory," Opt. Eng. **36,** 2737–2746 (1997).
23. J. Rosen, "Three-dimensional electro-optical correlation," J. Opt. Soc. Am. A **15,** 430–436 (1998).
24. J. Rosen, "Three-dimensional joint transform correlator," Appl. Opt. **37,** 7538–7544 (1998).
25. O. Matoba, E. Tajahuerce, and B. Javidi, "Real-time three-dimensional object recognition with multiple perspectives imaging," Appl. Opt. **40,** 3318–3325 (2001).